Coupled length scales in eroding landscapes

Kelvin K. Chan[†] and Daniel H. Rothman[‡]
Department of Earth, Atmospheric, and Planetary Sciences,
Massachusetts Institute of Technology, Cambridge, MA 02139

(Dated: November 14, 2000)

We report results from an empirical study of the anisotropic structure of eroding landscapes. By constructing a novel correlation function, we show quantitatively that small-scale channel-like features of landscapes are coupled to the large-scale structure of drainage basins. We show additionally that this two-scale interaction is scale-dependent. The latter observation suggests that a commonly applied effective equation for erosive transport may itself depend on scale.

PACS numbers: 92.40.Fb, 94.40.Gc, 05.65.+b, 45.70.Qj

Landscapes erode in part due to the shearing stresses imposed by the downhill transport of water, sediment, and other material [1]. Whereas the effects of erosion appear nearly obvious to the eye, they are notoriously hard to quantify. For example, the functional form of many river-network scaling laws [2] may be obtained from simple graphical constructions [3, 4] that have no obvious relation to real surfaces, eroded or not. Moreover, the appropriate partial differential equations for dynamic modeling are a source of much controversy [5–21]. Here we report results from analyses of eroded topography that explicitly quantify a unique aspect of landscape erosion—a coupling between small-scale channel-like features and the large-scale structure of drainage basins. A detailed study of this two-scale interaction reveals a rich hierarchy of scale dependencies in erosive processes. We provide evidence that these same scale dependencies are implicitly present in a commonly applied phenomenological theory of erosive transport [5–16].

We probe the detailed anisotropic correlations of a landscape $h(\mathbf{r})$, where h is elevation and $\mathbf{r}$ is position. Our analysis is inspired by recent theoretical results [19, 20] that point out the role of anisotropy in erosion and by recent empirical analyses of other pattern forming systems [22, 23]. We first form the function

$$w(\mathbf{x}, \phi;\, L_c) = e^{i\mathbf{k}_\phi \cdot \mathbf{x}}\, g(\mathbf{x}; L_c). \tag{1}$$

The function w is built from a modulated plane wave. The plane wave's angular orientation ϕ and wavelength λ_0 determine the wavevector

$$\mathbf{k}_\phi = \frac{2\pi}{\lambda_0}(\cos\phi, \sin\phi), \quad 0 \le \phi < 2\pi, \tag{2}$$

and the plane wave is modulated by a Gaussian taper g with standard deviation $L_c/4$:

$$g(\mathbf{x}; L_c) = L_c^{-2}\, e^{-8|\mathbf{x}|^2/L_c^2}. \tag{3}$$

We correlate w with the local topography over a region of size L_c by computing

$$R(\mathbf{r}, \phi; L_c) = \left| \int_{|\mathbf{x}-\mathbf{r}| \le L_c/2} \mathrm{d}\mathbf{x}\, w(\mathbf{x}-\mathbf{r}, \phi; L_c)\, h(\mathbf{x}) \right|. \tag{4}$$

We then define the local *channelization vector* $\mathbf{c}(\mathbf{r})$ from the phase of the π-periodic component of $R(\mathbf{r}, \phi)$, i.e.,

$$\mathbf{c}(\mathbf{r}) = [-\mathrm{Im}(Z), \mathrm{Re}(Z)], \qquad Z = \int_0^{2\pi} e^{-2\phi i}\, R(\mathbf{r}, \phi)\, \mathrm{d}\phi. \tag{5}$$

When topographic height-height correlations $\langle |h(\mathbf{x}) - h(0)|^2 \rangle$ are elliptically anisotropic, $\mathbf{c}$ should be perpendicular to the dominant local wavevector with magnitude $2\pi/\lambda_0$. In other words, when λ_0 is of the order of the width of channels, $\pm\mathbf{c}$ points in the direction in which they flow [24], and $|\mathbf{c}|$ is proportional to the channel depth.

To complete our description, we define the coarse-grained slope

$$\mathbf{s}(\mathbf{r}; L_s) = G^{-1} \int_{|\mathbf{x}-\mathbf{r}| \le L_s/2} \mathrm{d}\mathbf{x}\, g(\mathbf{x}-\mathbf{r}; L_s)\, \nabla h(\mathbf{x}) \tag{6}$$

where the normalization factor $G^{-1} = \int_{|\mathbf{x}| \le L_s/2} \mathrm{d}\mathbf{x}\, g(\mathbf{x}; L_s)$. We calculate the angular difference $\delta\theta$ between $\mathbf{c}$ and $\mathbf{s}$ and study the averaged quantity

$$\langle \cos^2 \delta\theta \rangle = \left\langle \left(\frac{\mathbf{c} \cdot \mathbf{s}}{|\mathbf{c}||\mathbf{s}|} \right)^2 \right\rangle \tag{7}$$

where $\mathbf{c}$ and $\mathbf{s}$ are measured at length scales L_c and L_s, respectively, and the angle brackets indicate spatial averaging. Equation (7) should be interpreted as the average

[†]Currently at Physics Department, Boston University; Electronic address: kechan@buphy.bu.edu
[‡]Author to whom correspondence should be addressed; Electronic address: dan@segovia.mit.edu; URL: http://segovia.mit.edu/

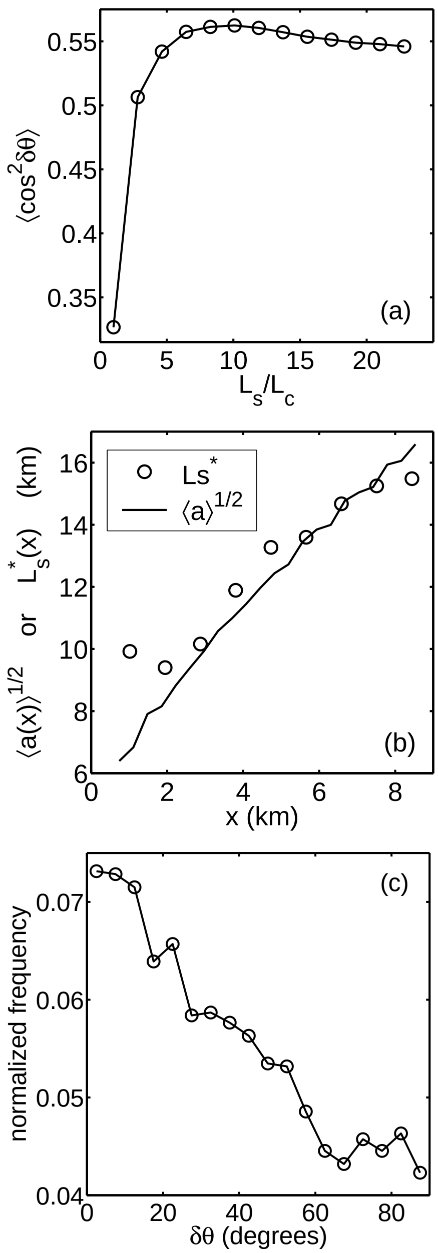

FIG. 1: (a) The mean squared cosine of the angular separation $\delta\theta$ between the slope vector $\mathbf{s}$ and the channelization vector $\mathbf{c}$ as a function of the ratio of the respective scales, L_s and L_c, at which they are calculated. Here $L_c = 1.0$ km and the maximum correlation occurs at $L_s^* \simeq 10L_c$. Curves computed for different values of L_c are qualitatively similar but the maximum occurs for a value L_s^* that depends on L_c. (b) Comparison between $L_s^*(L_c)$ (circles) and the square-root of the mean contributing area, $\langle a(b)\rangle^{1/2}$ (line), where both L_c and b are averaging lengths signified by x. (c) Histogram showing the frequency of occurrence of $\delta\theta$ for the case $L_c = 1.0$ km and $L_s = L_s^*$; i.e., the maximum correlation in (a).

correlation between a scale-dependent erosive response $\mathbf{c}(L_c)$ and a scale-dependent stress $\mathbf{s}(L_s)$ that induces it.

To see how these correlations manifest themselves in real topography, we have studied the USGS 1-degree digital elevation map that ranges from 38°–39° north latitude and 120°–121° west longitude, a rectangular area whose dimensions are roughly 100 km on a side, with a resolution of approximately 90 m. This area, entirely contained within California, ranges from the western flank of the Sierra Nevada mountains to the eastern edge of the Central Valley. A wide range of erosive features exist, including those of glacial, fluvial, and alluvial origin.

Figure 1a displays $\langle\cos^2\delta\theta\rangle$ as a function of L_s/L_c, averaged over the entire map. (Here and elsewhere, we study the case $\lambda_0 = 0.46$ km.) Although the correlations are never large, one striking feature stands out: the maximum occurs when $L_s \simeq 10\,L_c$, where here $L_c = 1.0$ km. In other words, the direction in which channel-like features flow locally is most strongly coupled to the direction of the topographic slope measured at a *much larger scale*. We call this large scale L_s^*. For any choice of L_c, a curve similar to that shown in Figure 1a is obtained, but with its maximum at a different L_s. Thus L_s^* is a function of L_c.

We next provide empirical evidence that L_s^* represents the average size of the individual basins that drain into a particular site on a map. Using the usual procedure [2], we calculate the area a_i that drains into the ith location. We calculate $\{a_i\}$ not only on the original map but also on maps coarse grained at a scale b. (Coarse graining is performed by computing the mean elevation in blocks of linear dimension b.) The average $\langle a(b)\rangle$ then represents the mean contributing area for the coarse-grained map, and a characteristic length scale may be obtained from its square root. Because both b and L_c are averaging length scales, we may compare $\langle a(b)\rangle^{1/2}$ to $L_s^*(L_c)$ for $b = L_c$. Figure 1b shows that the quantitative agreement is surprisingly good.

Another view of the two-scale interaction is shown in Figure 1c, a histogram of $\delta\theta$, for the case $L_s = 10$ km and $L_c = 1$ km, i.e., the point which gives the maximum in Figure 1a. One sees that the maximum probability is for $\delta\theta \simeq 0$. In other words, the nonlocal coupling of the scales L_s and L_c results in a tendency, on average, for the channelization vector $\mathbf{c}$ and the slope vector $\mathbf{s}$ to be parallel, but only when $L_s \gg L_c$. Note that isotropic random topography would yield a flat histogram for any choice of L_s and L_c. Thus the results of Figure 1 may have some practical use in the identification of the effects of fluvial erosion in environments—such as Mars [25]—where the origin of channel-like features is unclear.

We may provide a more detailed view of the two-scale interaction by explicitly incorporating the drainage area a in our correlations. We include the mth moment of a

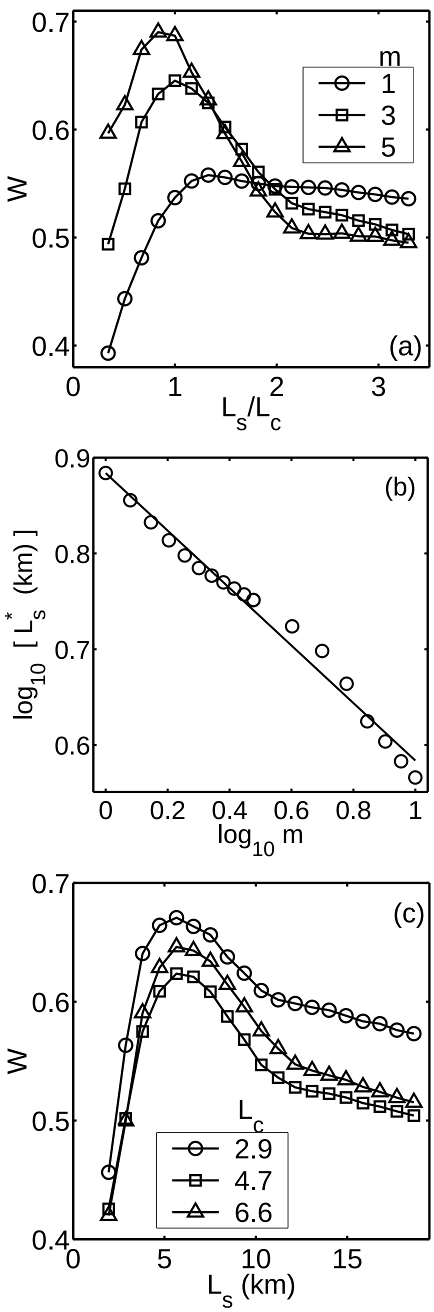

FIG. 2: (a) The correlation function W_m for the case $L_c = 5.7$ km, for $m = 1$ (circles), $m = 3$ (squares), and $m = 5$ (triangles). (b) Plot of $\log_{10} L_s^*$ as a function of the moment $\log_{10} m$ (circles), where L_s* is the value of L_s that maximizes W_m. The data are compared with a straight line of slope -0.3, indicating that L_s^* scales approximately as $m^{-0.3}$. (c) W_m as a function of L_s for $L_c = 2.9$ (circles), 4.7 (squares), and 6.6 km (triangles) for the case $m = 3$. A similar insensitivity of the shape and position of the curves with respect to L_c is found for other m.

in our measure of the locally averaged slope by defining

$$\tilde{\mathbf{s}}_m(\mathbf{r}; L_s) = G^{-1} \int_{|\mathbf{x}-\mathbf{r}| \le L_s/2} \mathrm{d}\mathbf{x}\, g(\mathbf{x}-\mathbf{r}; L_s)\, a^m(\mathbf{x})\, \nabla h(\mathbf{x}) \,. \tag{8}$$

We then compute the scale-dependent average

$$W_m = \frac{\langle |\mathbf{c} \cdot \tilde{\mathbf{s}}_m|^2 \rangle}{\langle |\mathbf{c}|^2 |\tilde{\mathbf{s}}_m|^2 \rangle} \tag{9}$$

where $\tilde{\mathbf{s}}_m$ and $\mathbf{c}$ are measured at scales L_s and L_c, respectively. The parameter m controls the statistical weight given to regions with large contributing area; the higher the moment m, the greater the weight given to slopes with large contributing area.

Figure 2a shows how W_m depends on L_s, L_c, and m. Three trends are worthy of note: (*i*) the maximum W_m^* of W_m increases with increasing m (Figure 2a); (*ii*) W_m^* occurs at a value L_s^* that decreases with m (Figures 2a and 2b); and (*iii*) $W_m(L_s)$ is insensitive to L_c (Figure 2c).

The first trend shows that, on average, $\mathbf{c}$ is most correlated with $\mathbf{s}$ when the drainage area is large. In other words, the two-scale interaction is strongest for channels that drain large basins. Recall additionally that $a(\mathbf{r})$ is a highly fluctuating function of space [2] (i.e., its variance is much larger than its mean), whereas $\mathbf{c}$ is not. The locations that contribute most to W_m are therefore where a is large. These locations become increasingly localized (i.e., they are less numerous, less distributed, and stronger) as m increases. Therefore the averaging scale L_s over which $\tilde{\mathbf{s}}_m$ correlates with $\mathbf{c}$ decreases with m, thus explaining the second trend. The third trend results from the slow variation of $\mathbf{c}$ compared to $\tilde{\mathbf{s}}_m$.

These results may provide some insight into phenomenological continuum-mechanical theories of erosion. Typically, these formulations assume, directly or indirectly, that the flux $\mathbf{j}$ of eroded material is proportional [26] to a product of drainage area and slope [5–16], i.e.,

$$\mathbf{j} \propto a^m s^n \hat{\mathbf{s}}, \tag{10}$$

where $s = |\mathbf{s}|$, $\hat{\mathbf{s}} = \mathbf{s}/s$, and n is another parameter. Our term $\tilde{\mathbf{s}}_m$ corresponds precisely to the right-hand side of (10) with $n = 1$, averaged over a scale L_s. Now assume that the left-hand side, when averaged over a scale L_c, may be approximated to first order by the channelization vector $\mathbf{c}$. (This assumption may be partially justified by noting that deeper channels carry more sediment.) In other words, we view $\tilde{\mathbf{s}}_m$ as a generalized force and $\mathbf{c}$ as an approximate flux. For this interpretation to be correct, $\tilde{\mathbf{s}}_m$ and $\mathbf{c}$ should be defined at the same scale L, and the maximum correlation W_m should occur at this scale. In Figure 2a these two conditions are satisfied by the curve W_3, which reaches its maximum at $L_s = L_c = 5.7$ km. Thus when the averaging scale $L = 5.7$ km, the "best" effective equation of the form (10) with $n = 1$ appears to require $m = 3$. More generally, since Figure 2c shows that W_m is independent of L_c, we may read directly from

Figure 2b that $L \simeq L_0 m^{-\alpha}$ with $L_0 \simeq 0.9$ km and $\alpha \simeq 0.3$, giving, upon inversion, $m \simeq (L/L_0)^{-1/\alpha}$.

The main conclusion to be derived from Figure 2 lies not with these specific numbers or relations but with the overall trend: small m characterizes large length scales, while large m characterizes small length scales. These observations are consistent with the notion that a diffusion equation [27] (corresponding to $m = 0$, $n = 1$) is a zeroth-order model of erosion. Higher powers of a in equation (10) then correspond to higher-order corrections that may be identified with smaller-scale features. Note, however, that our analysis provides no indication that these higher-order corrections become progressively smaller. Indeed, the trends in Figure 2a point in much the opposite direction.

Our results do not necessarily invalidate equation (10) as an effective transport law. Its use is often motivated by the observation that $\langle a^m s^n \rangle \simeq$ const. for an appropriate choice of m/n [2]. However Ref. [28] shows that $\langle a^m s^n \rangle \simeq$ const. also holds for random topography (i.e., Gaussian surfaces). Since random topography implies random $\mathbf{j}$, (10) cannot be valid for a random surface. Here, on the other hand, we find it invalid only in a scale-independent sense.

In conclusion, we have presented a multiscale analysis of an eroding landscape that explicitly quantifies the coupling of drainage basins to channels. This coupling has been shown to create a two-scale interaction which is itself scale dependent. These results indicate that a commonly employed effective equation for erosive transport also contains hidden dependencies on scale. While our results indicate that the construction of a comprehensive continuum theory for erosion is a formidable challenge, they do show one way in which landscape patterns of unknown origin [25] may be quantitatively analyzed to determine the kind of mechanisms that have eroded them. We hope that our methods may also find some applicability in the analysis of other types of landscapes—such as those formed by fracture [29]—where the underlying dynamics are poorly understood.

ACKNOWLEDGMENTS

We thank P. Dodds, R. Pastor-Satorras, A. Rinaldo and N. Schorghofer for helpful discussions. This work was supported in part DOE grant DE FG02-99ER 15004 and NSF grant EAR-9706220.

REFERENCES

[1] A. E. Scheidegger, *Theoretical Geomorphology* (Springer-Verlag, New York, 1991), 3rd ed.
[2] I. Rodríguez-Iturbe and A. Rinaldo, *Fractal River Basins: Chance and Self-Organization* (Cambridge University Press, Cambridge, 1997).
[3] R. L. Shreve, Journal of Geology **74**, 17 (1966).
[4] J. W. Kirchner, Geology **21**, 591 (1993).
[5] M. J. Kirkby, in *Slopes: Form and Process*, edited by M. J. Kirkby (Institute of British Geographers, London, 1971), pp. 15–29.
[6] T. R. Smith and F. P. Bretherton, Water Resources Research **3**, 1506 (1972).
[7] A. D. Howard and G. Kerby, Geological Society of America Bulletin **94**, 739 (1983).
[8] G. Willgoose, R. L. Bras, and I. Rodríguez-Iturbe, Water Resources Research **27**(7), 1671 (1991).
[9] D. S. Loewenherz, Journal of Geophysical Research **96**, 8453 (1991).
[10] A. D. Howard, Water Resources Research **30**, 2261 (1994).
[11] A. D. Howard, W. E. Dietrich, and M. A. Seidl, Journal of Geophysical Research **99**, 13,971 (1994).
[12] N. Izumi and G. Parker, J. Fluid Mech. **283**, 341 (1995).
[13] A. Giacometti, A. Maritan, and J. R. Banavar, Phys. Rev. Lett. **75**, 577 (1995).
[14] E. Somfai and L. M. Sander, Phys. Rev. E **56**, R5 (1997).
[15] J. R. Banavar, F. Colaiori, A. Flammini, A. Giacometti, A. Maritan, and A. Rinaldo, Phys. Rev. Lett. **78**, 4522 (1997).
[16] A. Giacometti, Phys. Rev. E **62**, 6042 (2000).
[17] S. Kramer and M. Marder, Phys. Rev. Lett. **68**, 205 (1992).
[18] D. Sornette and Y.-C. Zhang, Geophys. J. Int. **113**, 382 (1993).
[19] R. Pastor-Satorras and D. H. Rothman, Phys. Rev. Lett. **80**, 4349 (1998).
[20] R. Pastor-Satorras and D. H. Rothman, J. Stat. Phys. **93**, 477 (1998).
[21] P. S. Dodds and D. H. Rothman, Annu. Rev. Earth Planet. Sci. **28**, 571 (2000).
[22] C. Bowman and A. C. Newell, Rev. Mod. Phys. **70**, 289 (1998).
[23] D. A. Egolf, I. V. Melnikov, and E. Bodenschatz, Phys. Rev. Lett. **80**, 3228 (1998).
[24] Because the phase of $R(\phi)$ may be determined only within a multiple of π, the sign of $\mathbf{c}$ cannot be uniquely determined. Thus $\mathbf{c}$ is a *director* rather than a vector.
[25] M. H. Carr, *Water on Mars* (Oxford University Press, Oxford, 1992).
[26] Refs. [9, 10, 12] augment equation (10) with a threshold condition.
[27] W. E. H. Culling, J. Geol. **68**, 336 (1960).
[28] N. Schorghofer and D. H. Rothman, Phys. Rev. E (2001), to be published, cond-mat/0009383.
[29] J. M. Lopez and J. Schmittbuhl, Phys. Rev. E **57**, 6405 (1998).